Appl Microbiol Biotechnol (2017) 101:4935–4949
DOI 10.1007/s00253-017-8226-4

From a metagenomic source to a high-resolution structure of a novel alkaline esterase

Mariana Rangel Pereira[1,2,3] · **Thaís Carvalho Maester**[2,3] · **Gustavo Fernando Mercaldi**[1,4] · **Eliana Gertrudes de Macedo Lemos**[3] · **Marko Hyvönen**[5] · **Andrea Balan**[6]

Received: 31 July 2016 / Revised: 27 February 2017 / Accepted: 5 March 2017 / Published online: 22 March 2017

Abstract Esterases catalyze the cleavage and formation of ester bonds and are members of the diverse family of α/β hydrolase fold. They are useful in industries from different sectors, such as food, detergent, fine chemicals, and biofuel production. In a previous work, 30 positive clones for lipolytic activity were identified from a metagenomic library of a microbial consortium specialized in diesel oil degradation. In this study, a putative gene encoding an esterase/lipase, denominated *est8*, has been cloned and the corresponding protein expressed recombinantly, purified to homogeneity and characterized functional and structurally. We show that the protein codified by *est8* gene, denominated Est8, is an alkaline esterase with high catalytic efficiency against *p*-nitrophenyl acetate and stable in the presence of up to 10% dimethyl sulfoxide. The three-dimensional structure of Est8 was determined at 1.85-Å resolution, allowing the characterization of the substrate-binding pocket and features that rationalize the preference of Est8 for short-chain substrates. In an attempt to increase the size of ligand-binding pocket and enzyme activity against distinct substrates of long chain, we mutated two residues (Met^{213} and Phe^{217}) that block the substrate channel. A small increase in the reaction velocity for *p*-nitrophenyl butyrate and *p*-nitrophenyl valerate hydrolysis was observed. Activity against *p*-nitrophenyl acetate was reduced. The functional and structural characterization of Est8 is explored in comparison with orthologues.

Keywords Esterase · Metagenomic · Structure · Est8 · *p*-NP esters

Electronic supplementary material The online version of this article (doi:10.1007/s00253-017-8226-4) contains supplementary material, which is available to authorized users.

✉ Andrea Balan
abalan@usp.br

[1] National Laboratory of Biosciences (LNBio), Brazilian Center for Research in Energy and Materials (CNPEM), Campinas, São Paulo State, Brazil

[2] University of São Paulo (USP), São Paulo, São Paulo State, Brazil

[3] Department of Technology, São Paulo State University (UNESP), Jaboticabal, São Paulo State, Brazil

[4] Institute of Biology, University of Campinas, Campinas, São Paulo State, Brazil

[5] Department of Biochemistry, University of Cambridge, Cambridge, UK

[6] Department of Microbiology, Institute of Biomedical Sciences, University of São Paulo, São Paulo, Brazil

Introduction

Lipolytic enzymes are among the most useful biocatalysts with high potential to be employed in various industrial applications such as production of pure compounds (Lorenz and Eck 2005; Quax and Brokhuizen 1994), food processing (Giuliani et al. 2001; Choi and Lee 2001), paper (Kontkanen et al. 2004), and detergent manufacturing (Jaeger and Reetz 1998). These enzymes are widely distributed in animals, plants, and microorganisms and are classified according to their substrate preference as either esterases (E.C.3.1.1.1) or lipases (E.C.3.1.1.3), both of which catalyze the hydrolysis and synthesis of fatty acid esters (Arpigny and Jaeger 1999).

Esterases and lipases are members of a diverse family of α/β hydrolases (Nardini and Dijkstra 1999) that have diverged from a common ancestor preserving the arrangement of the catalytic residues but not the binding site as a whole (Ollis et al. 1992). Esterases can be differentiated from lipases by the nature of their preferred substrates and interfacial activation, substrate hydrophobicity, enantioselectivity, and

solvent stability (Bornscheuer 2002). Bacterial lipolytic enzymes have been traditionally classified into eight families based on their biological properties and conserved sequence motifs (Arpigny and Jaeger 1999), but new families have recently been proposed (Lee et al. 2006; Kim et al. 2009; Rao et al. 2013).

Several lipolytic enzymes from family IV have been isolated from different environments through metagenomic approach (JunGang et al. 2010; Jeon et al. 2012; Jin et al. 2012; Peng et al. 2014). However, just a few of them have been functionally and structurally characterized (Byun et al. 2007; Nam et al. 2009; Ngo et al. 2013). In a previous publication (Pereira et al. 2015), we identified the PL17.E10 fosmid clone from a metagenomic library of a microbial consortium specialized for diesel oil degradation (Paixão et al. 2010), which showed strong lipolytic activity on agar Petri dishes containing tributyrin. The DNA of PL17.E10 was subcloned, sequenced, and annotated. Four open reading frames (ORFs) were identified encoding putative α/β hydrolases, which may be responsible for the lipolytic activity. In addition, we showed that Est16 is one of these proteins, which belongs to family V of bacterial lipolytic enzymes, and it is active against a broad range of substrates with short and long acyl chains, mainly *p*-nitrophenyl butyrate (C_4) and *p*-nitrophenyl valerate (C_5) (Pereira et al. 2015). Similarly, Est3 was isolated from the same metagenomic library, belonging to family IV. It exhibited activity against C_4, C_5, and C_8 (Maester et al. 2016).

Following the identification of new enzymes with biotechnological application potential, this work shows that Est8 is another member of family IV of bacterial lipolytic enzymes sharing structural similarities with the highly thermostable esterase from *Pyrobaculum calidifontis* (PDB ID 2YH2) (Palm et al. 2011) but has preferential activity against short-chain substrates. The three-dimensional structure of the protein was solved by crystallography and compared with other esterases in terms of residues from the ligand-binding site, catalytic activity, and characteristics of internal cavity. We discuss key features required for enzyme selectivity and activity.

Material and methods

Screening for lipolytic activity

As described in a previous work (Pereira et al. 2015), a fosmid metagenomic library isolated from a microbial consortium specialized in diesel oil degradation was screened for potential esterases/lipases. Positive clones were selected based on their ability to hydrolyze tributyrin in Luria-Bertani (LB) agar Petri dishes evidenced by the formation of a clear halo around the colony. Positive clones were subcloned and their sequences were analyzed to identify putative esterases.

Sequence analysis of *est8* gene

Amino acid sequence of Est8 was used as a query sequence in a BLAST search at the National Center for Biotechnology Information (NCBI, Bethesda, Maryland, USA) for identification of orthologous proteins. Representative sequences belonging to eight families of bacterial lipolytic enzymes, as proposed by Arpigny and Jaeger (1999), and also proteins for which three-dimensional structures were available in the Protein Data Bank (PDB) were selected from the results of the BLAST search. A multiple sequence alignment was constructed in ClustalW algorithm (Thompson et al. 1994) in the BioEdit Sequence Alignment Program (version 7.0.5.3) using pairwise alignment with gap opening 35.00 and extension 0.75 and multiple alignments with gap opening 15.00 and extension 0.30. The alignment file was submitted to Mr. Bayes 3.2 (Ronquist et al. 2012) and MEGA 6.0 (Tamura et al. 2013) to estimate a suitable evolutionary model for phylogenetic tree construction. The tree was constructed using maximum likelihood method with a bootstrap of 1000 replicates and the Whelan and Goldman (WAG) matrix of amino acid substitution. Information of all sequences used in the alignment and phylogenetic tree are shown in Table S1 (Supplementary Information).

DNA amplification and plasmid construction

A DNA fragment of 936 base pairs containing the *est8* gene (GenBank accession no. KP699699) corresponding to entire 311 amino acid coding region was amplified by PCR from the positive clone Pl17.E10. The forward (5′ CGCGGAATTCACAATGGCACTCGATC 3′) and reverse (5′ CGGGAAGCTTCCTCACGCCAGCGCC 3′) oligonucleotides were used for the fragment amplification and insertion of the *Eco*RI and *Hin*dIII restriction enzymes sites (underlined), respectively, in the start and final of the gene. The PCR product was directly cloned into pET28a plasmid (Novagen, Gibbstown, NJ, USA) to generate the pET28a-*est8* vector. The expressed protein from this construct presented a N-terminal His-tagged for further purification, confirmed by DNA sequencing analysis. In order to open the substrate channel in Est8, we also amplified *est8* gene containing two point mutations in the Met213 and Phe217, which were replaced by Val and Gly, respectively. The mutagenesis was performed using two overlapping oligonucleotides (5′ GACGGCGTGATCTGGTTCGGCGATC 3′ and 5′ GATCGCCGAACCAGATCACGCCGTC 3′) that introduced the mutations in two steps of PCR reaction. Terminal oligonucleotides for final amplification (5′ TATATCCATGGCACTCGATCCGCAGGCAAAAG 3′ and 5′ TATATAAGCTTACGCCAGCGCCTCTTTCAGCGCCTTC 3′) introduced restriction sites for *Nco*I and *Hin*dIII, respectively (underlined). The mutated sequence was cloned into pHAT2

vector (Peränen et al. 1996), producing pHAT2-*est8mf* plasmid. The mutated protein is called Est8MF.

Protein expression, extraction, and purification

The recombinant plasmids were transformed into chemically competent *Escherichia coli* BL21(DE3) cells for overexpression. The transformed cells were grown in LB media containing kanamycin (50 μg mL^{-1}) or ampicillin (100 μg mL^{-1}) and agitated at 200 rpm at 37 °C until OD_{600} reached 0.5–0.6. Expressions of Est8 and Est8MF proteins were induced with 0.4 mM isopropyl β-D-1-thiogalactopyranoside (IPTG) from *E. coli* BL21 (DE3) cells, respectively, carrying pET28a-*est8* and pHAT2-*est8mf* vectors, and grown for further 18 h at 20 °C. After this, the cultures were centrifuged at 8000*g* for 10 min at 4 °C. The cells were resuspended in 30 mL of 50 mM Tris-HCl pH 8.0 and lysed with Emulsiflex C5 homogenizer (Avestin Inc., Canada). The cell lysates were adjusted to 500 mM NaCl, 10 mM imidazole, 10 mM (*v*/*v*) β-mercaptoethanol, and 10% (*v*/*v*) glycerol and centrifuged at 17,000*g* for 45 min at 4 °C to pellet the cell debris. The soluble fractions of the cell lysates were purified using immobilized metal ion chromatography with Ni-NTA resin. An imidazole gradient using the buffer 50 mM Tris-HCl pH 8.0, 500 mM NaCl, and 10% (*v*/*v*) glycerol was performed. Bound proteins were eluted in the same buffer containing 200 mM imidazole. Peak fractions were pooled, concentrated, and further purified using size exclusion chromatography (SEC) in a Superdex 200 HiLoad 16/60 column (GE Healthcare Bio-Sciences, Uppsala, Sweden) at room temperature in 20 mM Tris-HCl pH 8.0, 200 mM NaCl, and 5% (*v*/*v*) glycerol. The purified fractions of Est8 and Est8MF were analyzed by SDS-PAGE under denaturing conditions, concentrated, and stored at −80 °C.

Circular dichroism and spectroscopic analysis

To evaluate the stability of Est8 and Est8MF in different pH, we monitored the secondary structure content and the tryptophan environment using circular dichroism (CD) and intrinsic tryptophan fluorescence. Far-UV CD spectra were recorded on a Jasco-810 spectropolarimeter using a PFD 425S Peltier system for temperature control. Both Est8 and Est8MF proteins were prepared at the final concentration of 5.5 μmol in two different buffers, which are 5 mM sodium phosphate pH 7.0 and 5 mM N-cyclohexyl-2-aminoethanesulfonic (CHES) pH 9.0. For Est8MF, a CD spectrum was obtained in presence of 11 μmol of substrates *p*-nitrophenyl acetate (C_2) or *p*-nitrophenyl butyrate (C_4). All measurements were acquired at 10 °C using a 1-mm path length cell at 0.5-nm intervals over the wavelength range from 195 to 260 nm. The ellipticity was reported as the mean residual ellipticity $[\theta]_{MR}$ (deg cm^2 $dmol^{-1}$). Samples were also subjected to thermal unfolding from 20 to 110 °C with spectra collected at 1 °C intervals. The loss of secondary structure was examined by measuring the ellipticity at 222 nm. The T_m represents the temperature at the midpoint of the unfolding transition. All data collected were corrected for the buffer baseline contribution.

The fluorescence experiment of Est8 was performed at room temperature in K2 multifrequency cross-correlation phase and modulation fluorometer (ISS Inc., Champaign, IL, USA). Of the Est8, 1 μM was diluted in 5 mM Tris-HCl buffered at pH 7.0, 8.0, and 9.0. Assays using tributyrin as substrate were based on the stoichiometry of 1:2 (protein:ligand), and samples were incubated for 30 min at room temperature before measurements. Tryptophan fluorescence was measured with an excitation wavelength of 295 nm, and the emission spectra were recorded between 300 and 400 nm.

Enzymatic characterization of Est8

The enzymatic activity of purified Est8 was tested at different pHs (7.0, 8.0, and 9.0) on tributyrin-agar Petri dishes containing 0.23% (*w*/*v*) Tris, 1.2% (*w*/*v*) agar, and 1% (*v*/*v*) tributyrin. Est8 was prepared at a concentration of 50 μg mL^{-1} and 20 μL was added to each dish. The material was incubated at 37 °C for 1 day to verify the substrate hydrolysis and halo formation.

Kinetic parameters of Est8 activity were obtained by measuring the formation of *p*-nitrophenol after para-nitrophenol (*p*-NP) acyl ester hydrolysis. The reactions were measured against an enzyme-free sample that was used to subtract auto-hydrolysis, and the released *p*-nitrophenol was spectrophotometrically quantified at 405 nm using a 2104 Envision Multilabel Reader (PerkinElmer, Waltham, MA, USA). Absorbance readings were converted to *p*-NP concentration using molar absorption coefficient of $\varepsilon_{p\text{-}NP}$ = 17,000 M^{-1} cm^{-1}. All assays were measured in triplicates in 96-well plates with a final volume of 100 μL, using JANUS Varispan automated liquid handler for plate preparation (PerkinElmer). Unless otherwise indicated, the reactions were developed at 25 °C using 1 nM of the enzyme, 1 mM of substrates in 50 mM Tris-HCl pH 8.0, and with 0.3% (*v*/*v*) Triton X-100. The enzyme activity was tested against different *p*-NP acyl esters [acetate (C_2), butyrate (C_4), and valerate (C_5); Sigma, San Louis, MO, USA]. The optimum temperature for Est8 activity was evaluated with *p*-NP acetate, and the measurements were performed in EnSpire Plate Reader (PerkinElmer), configured to make a temperature ramp from 25 to 55 °C. The pH optimum of Est8 was investigated using different buffering agents to establish a pH range from 5 to 10 (sodium citrate pH 5.0 and 6.0; Tris-HCl pH 7.0, 8.0, and 9.0; and CHES pH 10.0). These reactions were performed with *p*-NP acetate as substrate.

Est8 activity was tested in the presence of salts, metal ions, detergents, and solvents against *p*-NP acetate. The influence of metals (Zn^{2+}, Ni^{2+}, Mn^{2+}, Mg^{2+}, K^{+}, Co^{2+}, and Ca^{2+}) was measured in the presence of 0.5 mM of each reagent and in the absence of them as a control. Est8's tolerance towards detergents and solvents was tested in the presence of Tween 20 or Triton X-100 [0.3125 to 5% (*v*/*v*)], dimethylformamide (DMF), or dimethyl sulfoxide (DMSO) [2.5 to 10% (*v*/*v*)]. Control samples were prepared in the same conditions without detergents and solvents. The kinetic parameters were performed using 1 nM of Est8 and *p*-NP acyl esters at concentration varying from 0.078 to 1 mM at 25 °C. The catalytic rate constant (K_{cat}) was calculated from the initial steady-state velocity according to the equation $K_{cat} = V_{max}/[E]$. The data from functional characterization of Est8 was analyzed using the R software. ANOVA and Tukey's test at 5% probability were used to make comparisons among the different conditions evaluated.

Est8 crystallization

Initial crystallization trials were performed in 96-well plates with 100 and 200 nL drop sizes using the following commercial kits: Crystal Screen and SaltRx (Hampton Research, Aliso Viejo, USA), JCSG suite and PACT suite (Qiagen, Hilden, Germany), and Precipitant synergy and Wizard I and II (Emerald BioSystems, Bainbridge Island, WA, USA). First crystals were obtained in 2% (*v*/*v*) polyethylene glycol (PEG) 8000 and 0.8 M triammonium citrate pH 8.5; this condition was refined by varying salt, protein concentrations, and pH. Optimization plates were prepared manually through vapor-diffusion technique using 1:1- and 1:0.5-μL ratios of protein and mother liquor and incubated at 18 °C. Crystals were cryo-protected with 20% (*v*/*v*) glycerol in mother liquor and cryo-cooled in liquid N_2.

Data collection, processing, and structure refinement

Diffraction data from cryo-cooled crystals were collected at the beamline I02 from Diamond Light Source, Oxfordshire, UK, using a Pilatus 6M detector. Datasets of Est8 were indexed and integrated using XDS (Kabsch 2010). The structure was solved by molecular replacement using Phaser program in CCP4 package (Winn et al. 2011) with *Alicyclobacillus acidocaldarius* carboxylesterase as a template model (PDB ID 1EVQ), which shares 43% of amino acid sequence identity with Est8. The structure was refined using REFMAC5 (Murshudov et al. 2011) and phenix. Refine programs and model were corrected manually using COOT (Emsley and Cowtan 2004). Analyses of the structures and figures were made with PyMOL (Delano 2010). All statistics from data collection and refinement are shown in Table S2 (Supplementary Information).

Data bank accession codes

The DNA sequence of *est8* gene was deposited at NCBI under the accession number KP699699, and the coordinates and structure factors of Est8 were deposited in the PDB under accession code 4YPV.

Results

Est8 is a family IV member of esterases and lipases

We screened our metagenomic library for esterases using colony assay on tributyrin containing agar plates. From the 30 clones that showed lipolytic activity, PL17.E10 clone was selected for sublibrary construction (Pereira et al. 2015). The gene annotation was carried out, and ORF8, which consists of 936 bp (311 amino acids), was selected for further analysis among 25 ORFs. Its deduced amino acid sequence was submitted to BLASTp analysis at the NCBI, using the non-redundant protein sequence (nr) database, and showed 72% identity with an α/β hydrolase protein from *Parvibaculum lavamentivorans* (GenBank accession no. WP012110575.1) and 65% identity with a carbohydrate esterase from *Phaeomarinobacter ectocarpi* (GenBank accession no. CDO59205.1). Moreover, against the metagenomic protein (env_nr) database, Est8 showed 52% identity with hypothetical proteins from marine (GenBank accession no. EDJ20548.1) and freshwater metagenome (GenBank accession no. KGA15039.1), respectively.

To establish the phylogenetic relationships of Est8 within eight families of bacterial lipolytic enzymes as proposed by Arpigny and Jaeger (1999) and with esterases/lipases with known structure, a phylogenetic tree was built from selected sequences (Fig. 1a). The result evidenced that Est8 belongs to the same branch as two previously described members from family IV, which are *Cupriavidus necator* (GenBank accession no. AAC41424.1) and *Pseudomonas* sp. (GenBank accession no. AAC38151.1). The structurally defined member of this family is *P. calidifontis* esterase (PDB ID 2YH2) (Palm et al. 2011), an enzyme that converts esters in acids and alcohols and showed high structural conservation with Est8 three-dimensional structure as evidenced by the lowest values of root-mean-square deviation (Fig. 1b). Structural superposition between Est8 and other representative members from each family also evidenced close structural relationship with families V and VI. As shown in the multiple sequence alignment (Fig. 1c), all the proteins shared conserved sequence motifs characteristic of family IV, also known as hormone-sensitive lipase (HSL) family, confirming the phylogenetic tree results. The conserved residues from the catalytic triad Ser^{159}-Asp^{253}-His^{283} were identified, which nucleophile Ser is positioned in the consensus pentapeptide motif

GDSAG. The strictly conserved HGGG motif (H^{85}-G^{86}-G^{87}-G^{88}) is located upstream of Est8 active site (Fig. 1c, in green).

Kinetic characterization of Est8

Recombinant Est8 protein was expressed with the expected molecular mass of 37 kDa as calculated from its amino acid sequence and purified in two steps using a combination of Ni-NTA affinity and size exclusion chromatographies (Fig. S1-a, b, respectively, Supplementary Information). The pure Est8 protein was recovered from second peak of the size exclusion chromatography with a final yield of 110 mg mL^{-1} per liter of induced culture. The protein remained stable even at high concentrations (10–20 mg mL^{-1}) and during prolonged storage at 4 °C.

Purified Est8 was submitted to circular dichroism analysis in neutral (pH 7.0) and basic (pH 9.0) conditions. The CD spectra obtained showed a typical mixed α/β spectrum with minima at 208 and 222 nm, as expected for esterases/lipases (Nardini and Dijkstra 1999). Moreover, the spectra revealed that the pH tested did not alter the secondary structure (Fig. S1-c, Supplementary Information) or the denaturing temperature (Fig. S1-d, Supplementary Information) of Est8. Thermal denaturation of Est8 using CD showed a T_m of 55 °C (±1 °C).

Enzymatic analysis of Est8 showed that the enzyme was able to hydrolyze a very restricted range of substrates as *p*-NP acetate (C_2), *p*-NP butyrate (C_4), and *p*-NP valerate (C_5) (Fig. 2a), which is in accordance with its denomination as an esterase (Jaeger et al. 1999). Est8 revealed the highest efficiency catalytic against C_2 when compared with other esterases described in literature, as AFEST (Chahinian et al. 2005), EstFa_R (Ohara et al. 2014), and E40 (Li et al. 2015) (Table 1); furthermore, there is a greater catalytic efficiency for all substrates when compared to RmEstA esterase (Liu et al. 2013). Reactions against substrates with acyl esters with long-chain length [*p*-NP decanoate (C_{10}) to *p*-NP palmitate (C_{16})] were performed but no activity was detected.

Based on the results of the analysis of substrate specificity, *p*-NP acetate was chosen for all the further analyses. Est8 is a mesophilic enzyme that presented optimum activity at 30 °C, but showed relative activity above 43% in temperatures up to 55 °C (Fig. 2b), in accordance with its T_m of 55 °C evidenced in the CD analysis (Fig. S1-d, Supplementary Information). Est8 showed the maximum activity at pH 9.0 (Fig. 2c) and showed significant quenching of tryptophan fluorescence in presence of tributyrin as shown in Fig. 2d, e. At pH 9.0, besides the quenching, a displacement of the maximum peak of the spectrum to 320 nm is observed. These data are in accordance with the results presented for Est8 in Petri dishes plates that evidenced activity of the protein in basic pH (Fig. 2f).

In the presence of metal ions, the activity of Est8 showed no significant difference compared to the control, except for Zn^{2+}, Ni^{2+}, and Co^{2+} that reduced the activity to 3.9, 73.9, and 74.9, respectively (Fig. 2g). In the presence of increased concentrations of DMSO, the enzyme activity was similar to the one found in the control (up to 10% of this solvent) and still showed 65% of relative activity in the presence of 10% DMF (Fig. 2h).

In presence of detergents (Triton X-100, NP-40, and Tween 20), the enzyme activity is gradually reduced down to 27% of basal activity at the highest (5%) tested detergent concentration (Fig. 2i).

Crystallization and structure determination

Est8 crystal growth occurred until 6 days leading to bi-pyramidal crystals with dimensions ranging from 100 to 500 μm. Crystals were obtained in different crystallization conditions containing different polyethylene glycols and either 2-(N-morpholino)ethanesulfonic acid (MES) or 4-(2-hydroxyethyl) piperazine-1-ethanesulfonic acid (HEPES) buffers in pH 6.5–7.5. Refinement of all crystallization conditions lead to crystals grown in 1% (*v*/*v*) PEG 8000, 1.4 M triammonium citrate pH 9.0 using 17.8 mg mL^{-1} of pure protein, which diffracted at maximum of 1.85-Å resolution at Diamond Light Source. The data collected from Est8 crystals showed the symmetry and systematic absences of the primitive hexagonal space group $P3_12_1$. The Matthews coefficient was 3.35 $Å^3$/Da, and the solvent content 63.4% correspond to estimated one Est8 molecule in the asymmetric unit. The structure was solved using molecular replacement using *A. acidocaldarius* carboxylesterase (43% sequence identity) as a search model. The structure was refined and manually corrected resulting in a model with good stereochemistry and refinement statistics. Table S2 (Supplementary Information) summarizes the data collection and refinement statistics.

The refined structure of Est8 displays the conserved structure of esterases from the HSL family that shows an ellipsoidal shape defined by an α/β hydrolase fold, in which two domains can be identified, which are a globular catalytic domain and a helical cap domain that covers the entrance to the active site (Fig. 3a, green/orange and pale yellow, respectively). The catalytic domain has a mixed β-sheet composed of eight β-strands (only strand β2 is antiparallel) surrounded by the following ten helices: Pro^5-Ala^{16}, Ile^{22}-Asp^{24}, Val^{27}-Leu^{41}, Thr^{96}-Ala^{108}, Ala^{127}-Ile^{146}, Ala^{160}-Ala^{175}, Ala^{197}-Asn^{202}, Arg^{210}-Tyr^{220}, Leu^{255}-Ala^{269}, and

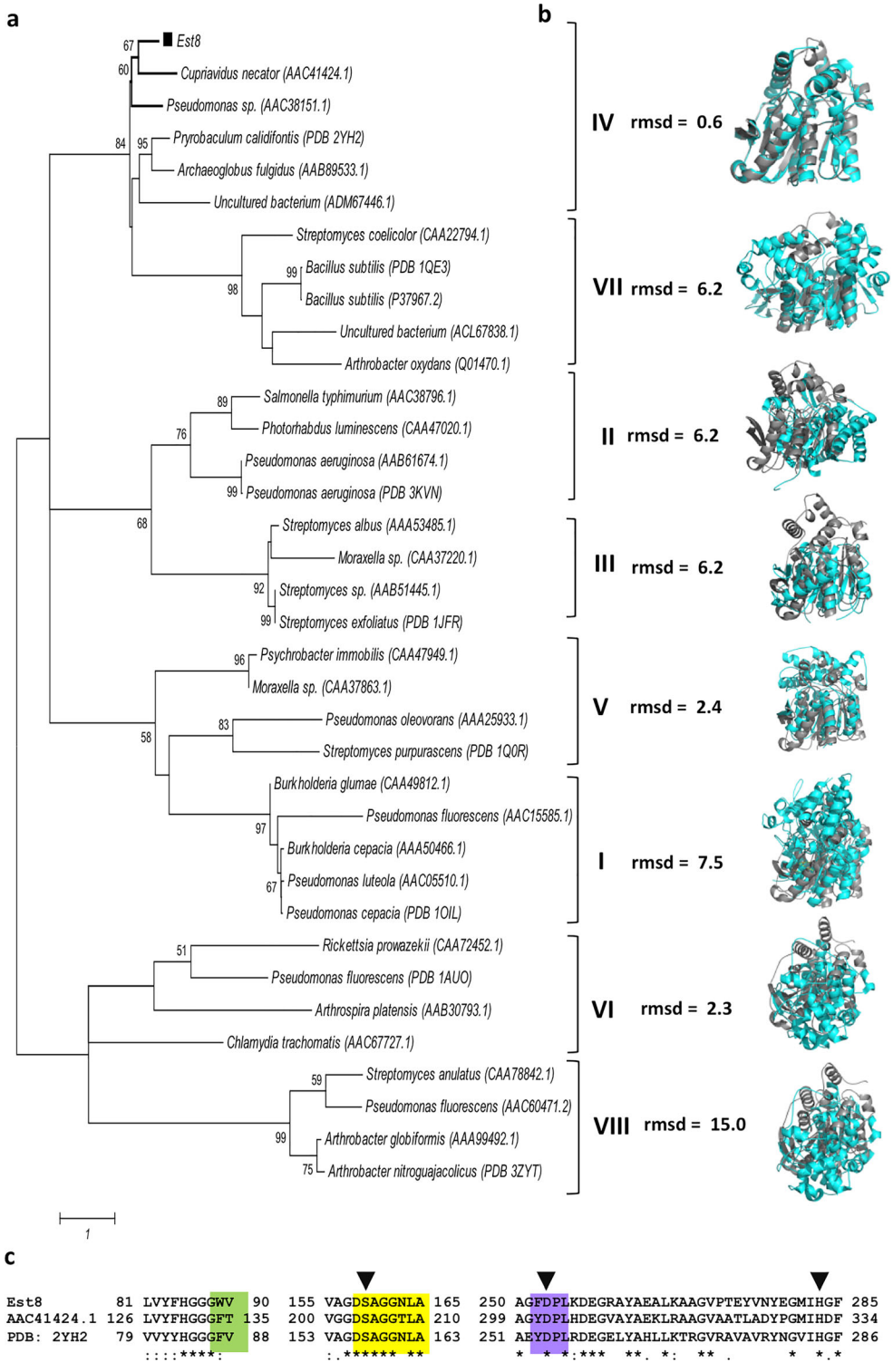

Asp[293]-Leu[310]. The cap domain that in orthologues controls the substrate entry and access to the active binding pocket is composed of Pro[5]-Pro[26] and Arg[210]-Leu[221] (Fig. 4a, pale yellow). The superpositioning of the three-dimensional structures of Est8 and the *P. calidifontis* esterase revealed a high conserved α/β-fold (root-mean-square deviation (rmsd) of 0.6 Å) (Fig. 3b) and identical positioning of the catalytic triad residues (Fig. 3c, cyan stick).

The catalytic nucleophile Ser[159] is positioned between β5 and α6, in the consensus pentapeptide motif GDSAG (Fig. 3c, yellow cartoon), while the other two

◀ **Fig. 1** Phylogenetic analysis of Est8 and sequence comparison with orthologues. **a** Phylogenetic tree of Est8. Representative members of eight bacterial lipolytic families and representative structurally characterized members for each class are shown. Accession numbers at NCBI database (for sequences) or PDB (for structures) are shown in parenthesis after the enzyme name. Multiple sequence alignment was performed with ClustalW and used as input for building the phylogenetic tree in MEGA 6.0 program based on the maximum likelihood method with a bootstrap of 1000 replicates. The estimated value of the shape parameter for the discrete gamma distribution was 11.9665. Substitution pattern and rates were estimated under the WAG model (+G + F) with two categories. Scale bar number of amino acids substitutions per site. **b** Structural differences between Est8 and members of each family shown by the rmsd. values obtained after the structural superposition. Est8 and one PDB member identified in the tree are, respectively, shown in gray and cyan cartoon. Members of family IV and V show the highest structural similarity with Est8. **c** Amino acid sequence alignment of Est8, *Cupriavidus necator* lipase (accession number AAC41424.1) and *Pyrobaculum calidifontis* esterase (PDB ID 2YH2), proteins classified in branch of family IV and their functional motifs. Amino acids that belong to the catalytic triad are indicated by arrow (black inverted triangle), and characteristic motifs from family IV are *colored*. All the sequences used in this figure are described in Table S1 (Supplementary Information)

residues (Asp^{253} and His^{283}) are found between β7 and α9 and between β8 and α10, respectively (Fig. 3c, cyan stick). The three amino acids in the catalytic triad are in close proximity with the residues that are involved in the formation of oxyanion hole during catalysis such as the strictly conserved HGGG motif (Fig. 3c, green sticks) (Wei et al. 1999). Other motifs that are involved in catalytic mechanism in members of family IV esterases, such as ^{157}GXSXGGNL^{164} (yellow cartoon) and ^{253}DPXXD^{257} (blue cartoon), are evident in the structure.

Interestingly, although Est8 and *P. calidifontis* esterase belong to the same family and conserve exactly the same three-dimensional structure, when the ligand-binding pockets are compared, we observed quite different channels (Fig. 4a, b, shown in colored surface). In fact, a BLASTp using Est8 sequence versus the PDB returned five other esterases/lipases that share the same fold with slight differences but show different catalytic activities (Table 1). The three enzymes that only accept two carbon substrates [Est8, *Pseudomonas putida* ECU1011 esterase (4OB8), and heroin esterase (1LZL)] do not have extended channel as observed in the other enzymes that are capable of cleaving larger substrates (Fig. 4). These differences are likely to be important for the selectivity towards particular substrates. In the comparison with many of the other related esterases, Est8 has a relative small active site cavity, lacking the extended substrate channel, in line with the higher activity it demonstrates against *p*-NP acetate (C_2). This is similar to other esterases that prefer substrates with short acyl chain, as shown in Fig. 4c, d. In contrast, enzymes that have larger channels show significant activity also for substrates with longer acyl chains, such as *p*-NP butyrate (C_4), *p*-NP hexanoate (C_6), and *p*-NP octanoate (C_8) (Fig. 4b–f).

Comparison of Est8 with Est3 and Est16

The amino acid sequence identity shared by the enzymes with Est8 is 80 and 13%, respectively, for Est3 and Est16 (Fig. 5a). Structurally, the proteins show significant differences in the number and organization of the helices from the cap domains as evidenced in Fig. 5a (gray cartoon). Interestingly, even belonging to the same family and sharing 80% of amino acid sequence identity, we can observe that the channel for entrance and fitting of the substrate in Est3 and Est8 proteins are quite different. Est8 has a small cavity, Est3 a long channel, and Est16 shows a long cavity that is also more exposed (Fig. 5b). These structural features lead to the differences observed in the kinetic parameters that revealed a higher efficiency of Est8 against short chains, especially against C_2, while the two other enzymes cannot hydrolyze these substrates. On the other hand, the reduced cavity shown in Est8 must be one of the reasons for its absence of activity against C_8 (Fig. 5c).

The opening of the channel for substrate in Est8 is not enough to increase the catalytic parameters of the enzyme

Comparing Est8 active site cavity with structures of enzymes with open substrate-binding channel, we observed that the residues Met^{213} and Phe^{217} appear to block the channel, restricting the enzyme to accept only short-chain substrates. To verify if the opening of the channel would induce differences in the activity of the enzyme, we generated the mutations Met^{213}Gly and Phe^{217}Val (Est8MF). As we were unable to determine the structure of the mutant protein, to predict the effect of the mutations on the channel, we built a model of Est8MF based on the Est8 wild-type structure. As expected, the mutations are predicted to result in the opening of the channel (Fig. 6a, b). After induction of *E. coli* BL21 (DE3) cells carrying the vector pHAT2-*est8mf* and purification of the mutant protein, as described in the "Material and methods" section, the kinetics of Est8MF was performed. The mutations induced an increasing of fourfold and twofold in the activity of enzyme against the substrates *p*-NP butyrate (C_4) and *p*-NP valerate (C_5) (Fig. 6c), respectively, but drastically reduced the activity against *p*-NP acetate (C_2) as well (Table 1).

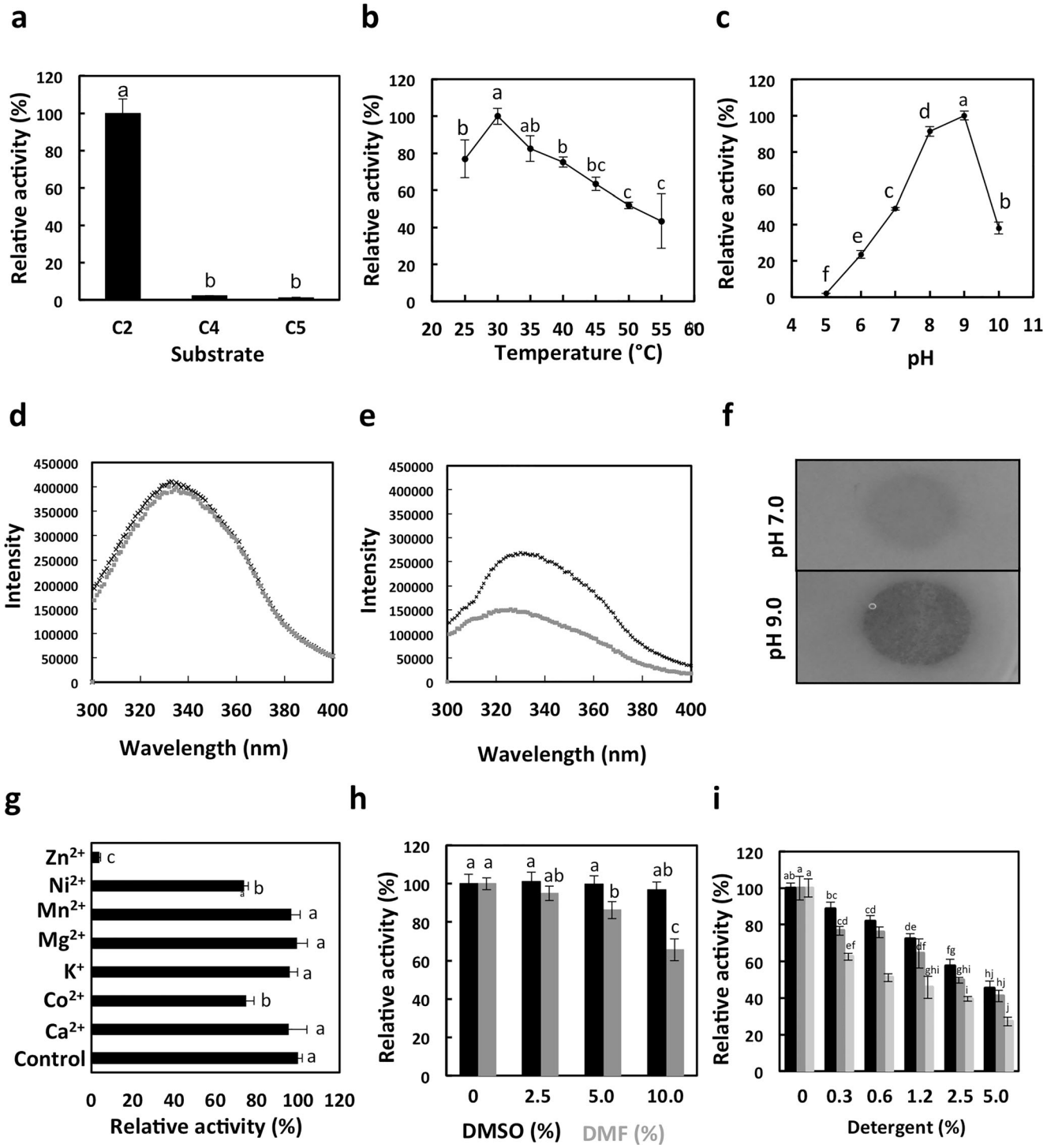

Fig. 2 Enzymatic characterization of Est8. **a** Substrate specificity of Est8 against *p*-nitrophenyl acetate (C_2), *p*-nitrophenyl butyrate (C_4), and *p*-nitrophenyl valerate (C_5). **b** The effect of temperature in the enzymatic activity using *p*-nitrophenyl acetate as a substrate with measures taken at every 5 °C from 25 to 55 °C. **c** The effect of pH on the enzymatic activity, measured on pH ranging from 5.0 to 10.0. **d** Tryptophan fluorescence spectrum of Est8 at pH 7.0 (*black line*) and 9.0 (*gray line*) in the absence of tributyrin. **e** Tryptophan fluorescence spectrum of Est8 at pH 7.0 (black line) and 9.0 (gray line) in the presence of tributyrin. **f** Agar containing 1% (*v*/*v*) tributyrin onto which 1 μM of Est8 has been spotted. The experiment was performed at room temperature, and a clear halo indicated esterase activity. **g** Influence of ions on Est8 activity. Control samples were prepared with no additives. **h** Influence of solvents. Black and dark gray bars correspond to DMSO and DMF, respectively. **i** Influence of detergents in the enzyme activity. Triton X-100 (black bar), NP-40 (dark gray bar), and Tween 20 (gray bar). All data are mean values of three independent measures, and the standard deviations are indicated by error bars. In the graphics (**a**–**c** and **g**–**i**), the small letters indicate the significant difference between each condition performed in the experiment, according to ANOVA and Tukey's test at 5% probability

Table 1 Kinetic parameters of Est8 and Est8MF and comparison with other esterases/lipases described in the literature

Protein	Description	Source	Substrate	K_{cat} (s^{-1})	K_m (mM)	K_{cat}/K_m (s^{-1} mM^{-1})	PDB code	Reference
Est8	Esterase	Metagenomic	*p*-NP acetate (C_2)	1,484 ± 52.6	0.224 ± 0.02	6,619.1	4YPV	This work
			p-NP butyrate (C_4)	23.72 ± 1.1	0.056 ± 0.01	425.03		
			p-NP valerate (C_5)	13.67 ± 0.52	0.245 ± 0.03	55.76		
Est8MF	Esterase	Metagenomic	*p*-NP acetate (C_2)	11.38 ± 1.68	0.125 ± 0.06	91.14	–	This work
			p-NP butyrate (C_4)	65.65 ± 2.27	0.745 ± 0.06	88.07		
			p-NP valerate (C_5)	25.27 ± 4.32	0.78 ± 0.25	32.39		
PestE	Esterase	*Pyrobaculum calidifontis*	*p*-NP propionate (C_3)	1,480 ± 110	0.348 ± 0.08	4,252.9	2YH2	Hotta et al. (2002)
			p-NP butyrate (C_4)	1,690 ± 20	0.164 ± 0.007	10,305		
			p-NP valerate (C_5)	2,070 ± 80	0.071 ± 0.01	29,155		
			p-NP caproate (C_6)	2,620 ± 90	0.044 ± 0.006	59,009		
			p-NP caprylate (C_8)	1,600 ± 270	0.051 ± 0.026	31,373		
HerE	Acetyl esterase	*Rhodococcus* sp.	6-acetylmorphine	12.6 ± 0.6	0.5 ± 0.06	25.2	1LZL	Zhu et al. (2003)
			phenyl acetate	3.0 ± 0.05	$7 \times 10^{-5} \pm 8 \times 10^{-6}$	42,857		
EstE1	Esterase	Metagenomic	Butyrate (C_4)	2,950	2.3	1,280	2C7B	Rhee et al. (2005)
			Valerate (C_5)	1,300	0.6	2,170		
			Caproate (C_6)	1,600	0.7	2,290		
AFEST	Carboxyesterase	*Archaeoglobus fulgidus*	Triacetin (C_2)	40	10	4	1JJI	Chahinian et al. (2005)
			Tripropionin (C_3)	110	0.3	366.67		
			Tributyrin (C_4)	95	0.05	1,900		
EstFa_R	Carboxylesterase	*Ferroplasma acidiphilum*	*p*-NP acetate (C_2)	13 ± 1	0.73 ± 0.12	17.8	3WJ2	Ohara et al. (2014)
			p-NP propionate (C_3)	28 ± 2	0.37 ± 0.07	74.4		
			p-NP butyrate (C_4)	56 ± 3	0.32 ± 0.05	173		
			p-NP caproate (C_6)	11 ± 1	0.13 ± 0.04	79.5		
RmEstA	Esterase	*Rhizomucor miehei*	*p*-NP acetate (C_2)	0.37	1	0.37	4WY5	Liu et al. (2012)
			p-NP butyrate (C_4)	1.17	0.17	6.90		
			p-NP hexanoate (C_6)	1.08	0.12	8.97		
			p-NP caprylate (C_8)	0.42	0.82	0.51		
			p-NP decanoate (C_{10})	0.04	0.28	0.13		
			p-NP laurate (C_{12})	0.02	3	0.06		
RmEstB	Esterase	*Rhizomucor miehei*	*p*-NP acetate (C_2)	0.195	1.6	0.122	4WY8	Yang et al. (2015)
			p-NP butyrate (C_4)	0.086	1.1	0.078		
			p-NP hexanoate (C_6)	0.031	5.6	0.005		
			p-NP caprylate (C_8)	0.019 0.004	4.7 6.5	0.004 0.0007		
E40	Esterase	Metagenomic	*p*-NP butyrate (C_4)	247	0.24	1,000	4XVC	Li et al. (2015)

C_2 *p*-NP-acetate, *C_3* *p*-NP-propionate, *C_4* *p*-NP-butyrate, *C_5* *p*-NP-valerate, *C_6* *p*-NP-caproate, *C_8* *p*-NP-caprylate, *C_{10}* *p*-NP-decanoate, *C_{12}* *p*-NP-laurate, *6-ACPA* acetyl morphine phenyl acetate

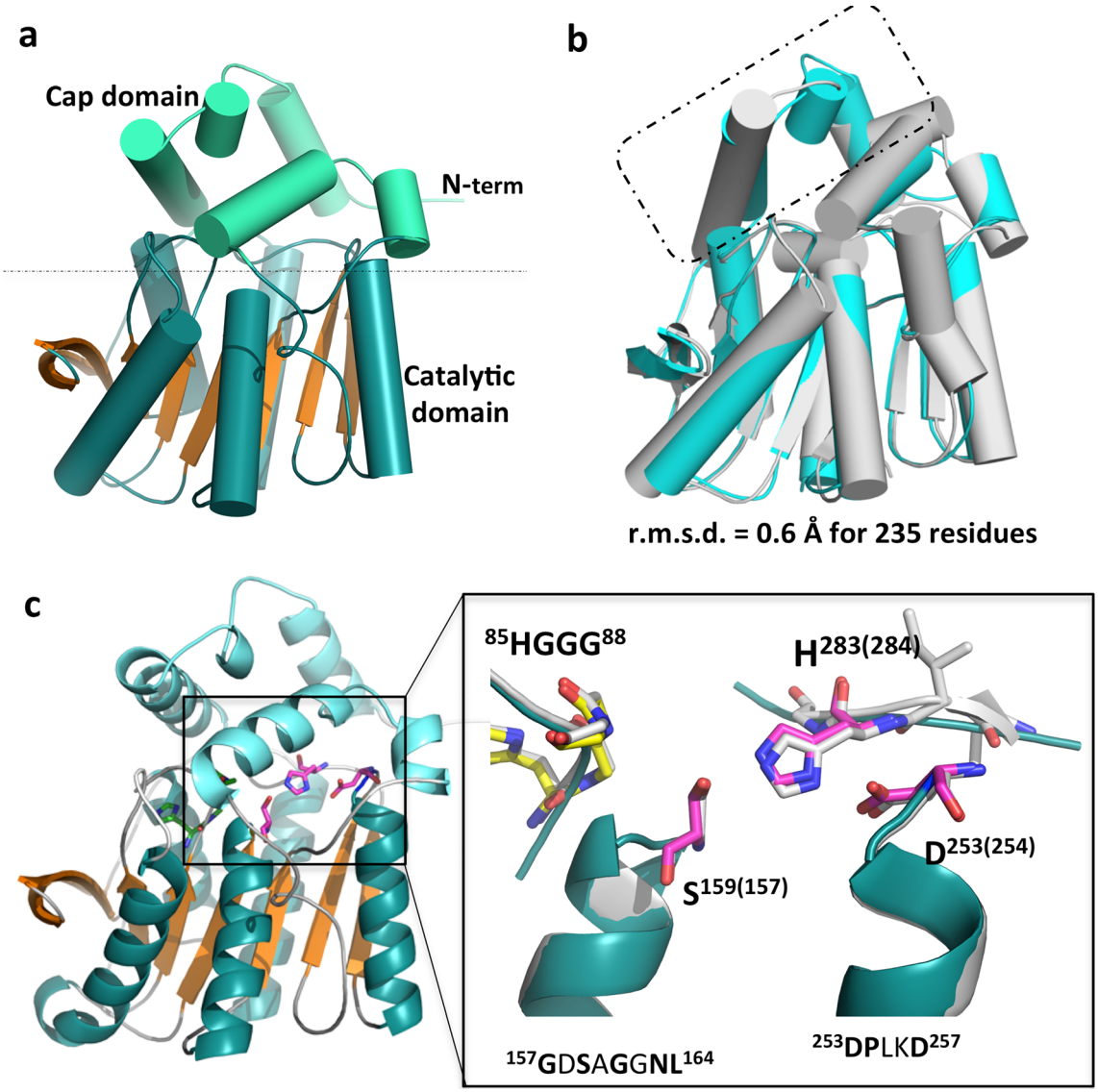

Fig. 3 Three-dimensional structure of Est8. **a** Cartoon representation of Est8 three-dimensional structure showing the cap domain (above the line) and catalytic domain (below the line). The catalytic domain consists of a β-sheet (orange) with eight β-strands surrounded by helices (cyan) forming a structure that sustains the active site. **b** Structural superposition of Est8 (cyan) and *Pyrobaculum calidifontis* esterase (PDB ID 2YH2; gray). The most significant difference in the cap domain is highlighted with a dotted rectangle. This structural feature is related to the accessibility to the active site and the volume of the enzyme pocket. The rmsd between both proteins is shown. **c** Overall positioning of the catalytic triad inside Est8 and detail of the superimposition of enzyme with the *P. calidifontis* esterase (residues shown in cyan stick). In Est8, the residues from the HGGG motif are shown in yellow, and those from catalytic triad are shown in pink stick

CD analyses revealed that Est8MF folding was not affected when compared to the wild type with slight differences in the helix content, as observed in the region 195 to 210 nm from the spectra (Fig. 6d). Similarly, the presence of substrates *p*-NP acetate (C_2) or *p*-NP butyrate (C_4) did not induce any difference in the folding of the mutant protein (Fig. 6e) but there is an increase of the T_m up to 4 °C, suggesting that the substrates help the protein stability (Fig. 6f).

Discussion

In this work, we showed the functional and structural characterization of Est8, a novel esterase isolated from oil-contaminated soil through metagenomic approach, in comparison with other orthologues previously characterized. The enzyme is a new member of family IV of bacterial lipolytic enzymes that showed stability in the

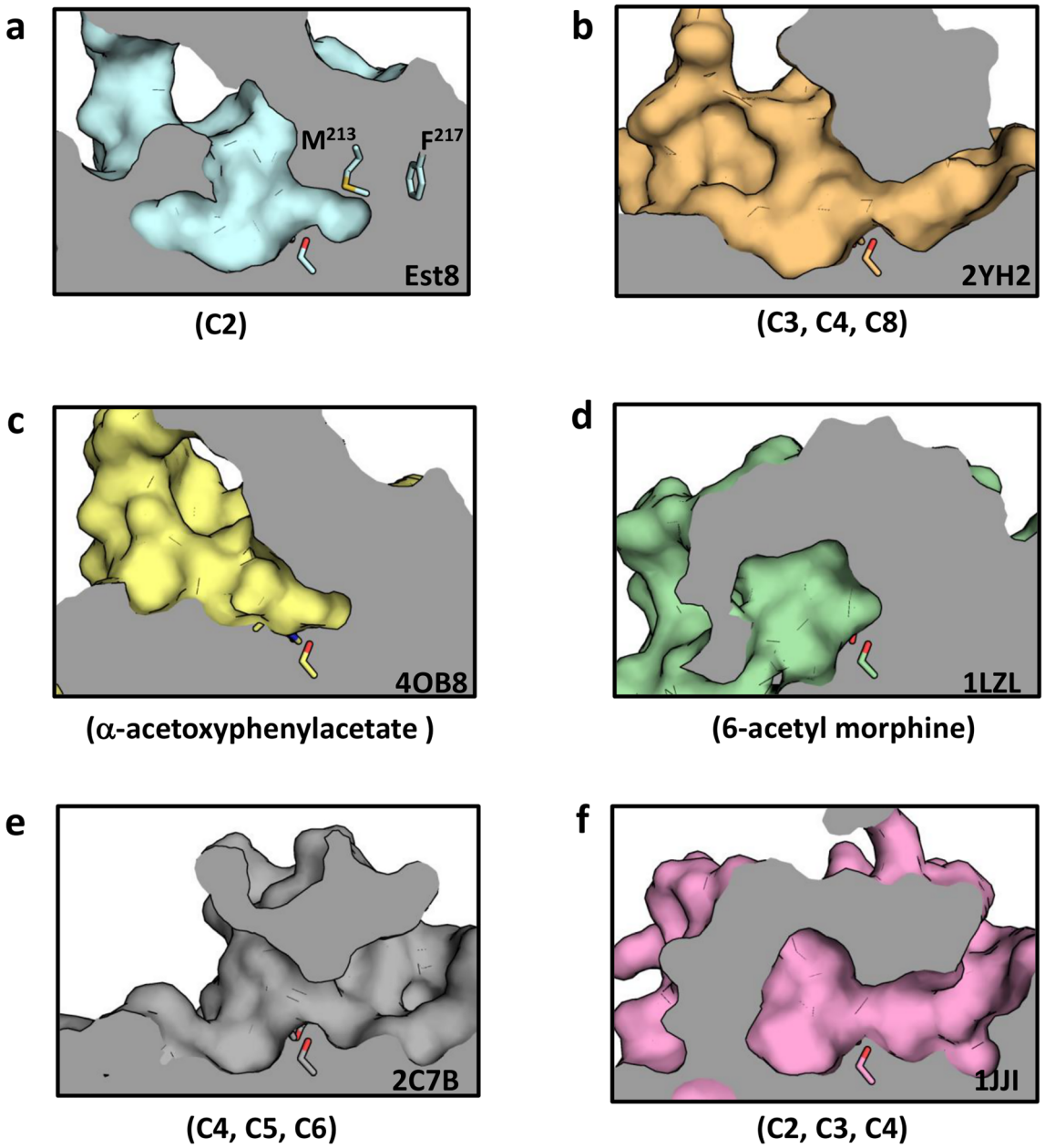

Fig. 4 Comparison of the substrate channel in different esterases/lipases that share similar fold with Est8. The figures show a cut-through of the structures with the gray surfaces show solid parts of the protein. On the other hand, the colored molecular surface lines show the active site cavities of the proteins. The enzymes are **a** Est8, **b** *Pyrobaculum calidifontis* esterase (PDB ID 2YH2), **c** *Pseudomonas putida* ECU1011 esterase (PDB ID 4OB8), **d** heroin esterase (PDB ID 1LZL), **e** ESTE1 carboxylesterase (PDB ID 2C7B), and **f** *Archaeoglobus fulgidus* carboxylesterase (PDB ID 1JJI). The best substrates for each enzyme are shown in parenthesis under the figures

presence of up to 10% (*v*/*v*) DMSO, optimum catalytic activity at 30 °C, highest efficiency catalytic against *p*-NP acetate, and melting temperature around 50 °C. Despite the structural conservation in members of family IV, we showed that the cap domain region in these proteins could be variable defining the cavity for substrate, the substrate range, and kinetic parameters. This observation is evidenced mainly when we compared structures belonging to the same family as Est8 and Est3 (Figs. 4 and 5). Even sharing 80% of identity, the differences in cap domain and cavity for substrate affect the pH range for activity (lower in Est3, pH 6 to

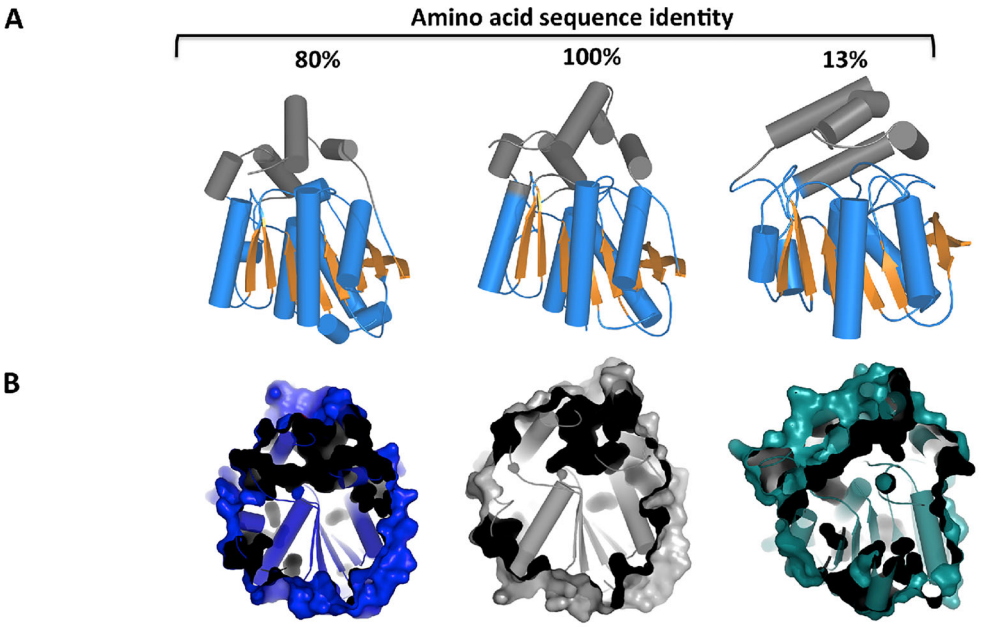

C

Substrates	Est3 K_{cat}/K_m ($min^{-1}.\mu M^{-1}$)	Est8 K_{cat}/K_m ($min^{-1}.\mu M^{-1}$)	Est16 K_{cat}/K_m ($min^{-1}.\mu M^{-1}$)
C2	-	397.15	-
C4	4.97	25.50	59.9
C5	4.96	3.34	39.9
C8	9.62	-	13.4

Fig. 5 Comparison among the enzymes Est8, Est3, and Est16. **a** Crystallographic structure of Est8 and the molecular models of Est3 and Est16 are shown in cartoon. The small domain or cap domain in HSL enzymes is shown in gray. Beta-sheet from the catalytic domains are shown in orange. The amino acid sequence identity is shown based on the Est8 protein. The models of Est16 and Est3 were built according to Pereira and collaborators (2015) and Maester and collaborators (2016), respectively. **b** Internal cavities or channels for substrate interaction showed in surface mode for the crystallographic structure of Est8 and molecular models of Est3 and Est16. The internal pockets are evidenced in *black*. All the structures are positioned in the same way with lateral view, cap domain in the up side and N terminal end on the right. **c** Comparison of the catalytic parameters of the enzymes against different substrates

8), substrates, and response to organic solvents and detergents (Maester et al. 2016). The small cavity evidenced by Est8 structure and the location of the nucleophile Ser^{159} in this cavity explain its selected high activity against C_2 shown in the kinetic analyses. In comparison with the *Rhizomucor miehei* esterase EstB (Rm EstB) (Yang et al. 2015), an enzyme that also showed high activity against C_2, Est8 is still more effective (Table 1). Similarly, both enzymes have small cavities constricted by the presence of aromatic residues that restrict carbon chain of long lengths, such as Met^{213} and Phe^{217} in Est8 and Trp^{92} and Phe^{222} in Rm EstB (Yang et al. 2015). In Est8, when mutations Met^{213}Gly and Phe^{217}Val were performed, changes in the previous steric hindrance led to an increasing of the relative activity against C_4 and C_5 as expected. However, the changes induced a dramatic effect in the activity against C_2, suggesting that the constricted acyl-binding site is important for the activity against this substrate.

Another important characteristic that might be interesting for industrial applications is the broad temperature range. Est8 was isolated from soils where the temperature usually gets more than 30 °C and showed relative activity of 40% for all temperatures up to 50 °C. Its mild thermal stability might be attributed to the fact that Est8 is a monomeric protein and does not present interactions between ion pairs in the catalytic domain, as pointed to be one of the essential factors for the stability in the monomeric enzyme Est2 from *A. acidocaldarius* (Manco et al. 2001). In hyperthermophilic enzymes, EstE1 from thermal environment (Byun et al. 2007), PestE from *P. calidifonti* (Mandrich et al. 2005), and Sto-Est from *Sulfolobus tokodaii* (Angkawidjaja et al. 2012) oligomerization is pointed as an important factor for stability due the increasing in the number of hydrogen bonds and hydrophobic interactions between the monomers. CD analyses revealed that there are no differences in the secondary structure content in different pH but there is a slight increase in the T_m at pH 9.0, the same pH where the protein suffered a pronounced quenching of tryptophans after addition of trybutyrin. This result suggests that in presence of the substrate, the protein could assume a more stable structure.

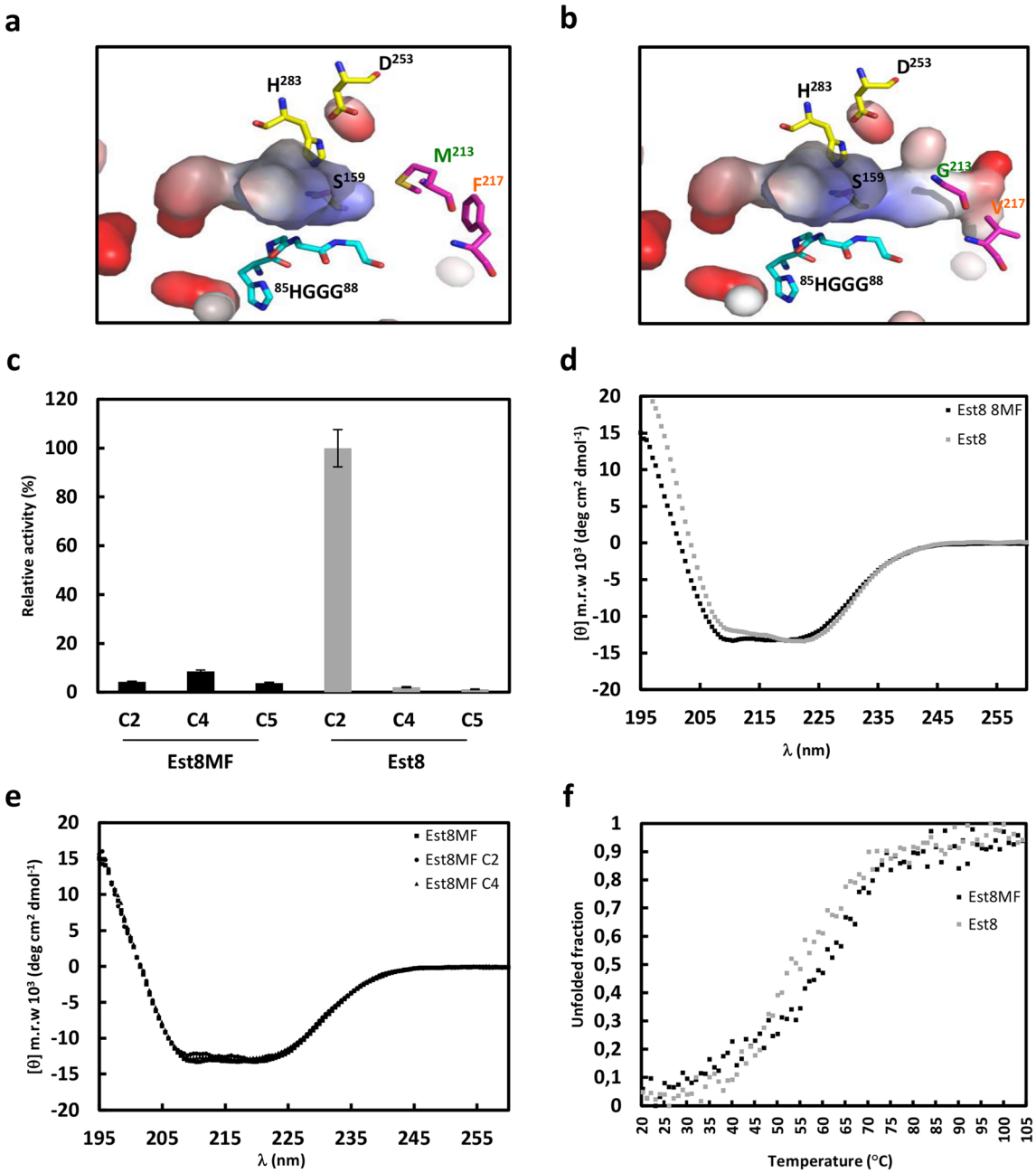

Fig. 6 Protein modeling and functional characteristics of Est8MF. **a** Est8 active site showing the residues Met^{213} and Phe^{217} that block the substrate channel. **b** Model of the opened channel in Est8MF. **c** Enzymatic activity of Est8MF compared to the wild type in presence of *p*-nitrophenyl acetate (C_2), *p*-nitrophenyl butyrate (C_4), and *p*-nitrophenyl valerate (C_5), **d** Circular dichroism spectra comparison between Est8 and Est8MF in Tris-HCl pH 8.0. **e** Circular dichroism spectra of 5.5 μmol Est8MF in presence and absence of substrates [11 μmol of *p*-nitrophenyl acetate (C_2) or *p*-nitrophenyl butyrate (C_4)]. The measurement was performed after 30-min incubation with the substrate at room temperature. **f** Thermal denaturation comparison between Est8 and Est8MF in pH 8.0

Finally, the results presented here show that Est8 is a new esterase isolated from metagenomic sources that present different characteristics when compared to orthologues previously described, including the two enzymes originated from the same habitat. Indeed, despite the fact that the enzyme did not show high thermal stability, it presented the highest activity against substrates of short chains, which could be explored for future applications such as production of milk fatty acid production.

Acknowledgements We are grateful for the Diamond Light Source for the provision of synchrotron radiation facilities, and we would like to thank the beamline managers for the assistance in using beamline I02

for data collection. We thank the infrastructure offered by the São Paulo State University (UNESP), Jaboticabal Campus, Brazil; the National Laboratory of Biosciences (LNBio), Campinas, Brazil; and the Department of Biochemistry, University of Cambridge.

Compliance with Ethical Standards

Funding This study was supported by São Paulo State Research Foundation (FAPESP), grant numbers 2011/09136-7 (PhD fellowship) and 2012/20490-0 (Research Internalships Abroad (BEPE)).

Conflict of interest The authors declare that they have no conflict of interest.

Ethical approval This article does not contain any studies with human participants performed by any of the authors.

References

Angkawidjaja C, Koga Y, Takano K, Kanaya S (2012) Structure and stability of a thermostable carboxylesterase from the thermoacidophilic archaeon *Sulfolobus tokodaii*. FEBS J 279: 3071–3084

Arpigny JL, Jaeger K-E (1999) Bacterial lipolytic enzymes: classification and properties. Biochem J 343:177–183

Bornscheuer UT (2002) Microbial carboxyl esterases: classification, properties and application in biocatalysis. FEMS Microbiol Rev 26:73–81

Byun J-S, Rhee J-K, Kim ND, Yoon J, Kim D-U, Koh E, Oh J-W, Cho H-S (2007) Crystal structure of hyperthermophilic esterase EstE1 and the relationship between its dimerization and thermostability properties. BMC Struct Biol 7:47–51

Chahinian H, Ali YB, Abousalham A, Petry S, Mandrich L, Manco G, Canaan S, Sarda L (2005) Substrate specificity and kinetic properties of enzymes belonging to the hormone-sensitive lipase family: comparison with non-lipolytic and lipolytic carboxylesterases. Biochim Biophys Acta 1738:29–36

Choi Y-J, Lee BH (2001) Culture conditions for the production of esterase from *Lactobacillus casei* CL96. Bioprocess Biosyst Eng 24:59–63

Delano WL (2010) The PyMOL molecular graphics system. Schrödinger LLC, New York

Emsley P, Cowtan K (2004) Coot: model-building tools for molecular graphics. Acta Crystallogr D Biol Crystallogr International Union of Crystallography 60:2126–2132

Giuliani S, Piana C, Setti L, Hochkoeppler A, Pifferi PG, Williamson G, Faulds CB (2001) Synthesis of pentylferulate by a feruloyl esterase from *Aspergillus niger* using water-in-oil microemulsions. Biotechnol Lett 23:325–330

Hotta Y, Ezaki S, Atomi H, Imanaka T (2002) Extremely stable and versatile carboxylesterase from a hyperthermophilic archaeon. Appl Environ Microbiol 68:3925–3931

Jaeger K, Reetz MT (1998) Microbial lipases form versatile tools for biotechnology. Trends Biotechnol 16:396–403

Jaeger K-E, Dijkstra BW, Reetz MT (1999) Bacterial biocatalysts: molecular biology, three-dimensional structures, and biotechnological applications of lipases. Annu Rev Microbiol 53:315–351

Jeon JH, Lee HS, Kim JT, Kim S-J, Choi SH, Kang SG, Lee JH (2012) Identification of a new subfamily of salt-tolerant esterases from a metagenomic library of tidal flat sediment. Appl Microbiol Biotechnol 93:623–631

Jin P, Pei X, Du P, Yin X, Xiong X, Wu H, Zhou X, Wang Q (2012) Overexpression and characterization of a new organic solvent-tolerant esterase derived from soil metagenomic DNA. Bioresour Technol 116:234–240

JunGang L, KeGui Z, WenJun H (2010) Cloning and biochemical characterization of a novel lipolytic gene from activated sludge metagenome, and its gene product. Microb Cell Factories 9:83–87

Kabsch W (2010) Xds Acta Crystallogr D Biol Crystallogr 66:125–132

Kim E-Y, Oh K-H, Lee M-H, Kang C-H, Oh T-K, Yoon J-H (2009) Novel cold-adapted alkaline lipase from an intertidal flat metagenome and proposal for a new family of bacterial lipases. Appl Environ Microbiol 75:257–260

Kontkanen H, Tenkanen M, Fagerström R, Reinikainen T (2004) Characterisation of steryl esterase activities in commercial lipase preparations. J Biotech 108:51–59

Lee M-H, Lee C-H, Oh T-K, Song JK, Yoon J-H (2006) Isolation and characterization of a novel lipase from a metagenomic library of tidal flat sediments: evidence for a new family of bacterial lipases. Appl Environ Microbiol 72:7406–7409

Li P-Y, Chen X-L, Ji P, Li C-Y, Wang P, Zhang Y, Xie BB, Qin QL, Zhou BC, Zhang YZ, Zhang XY (2015) Interdomain hydrophobic interactions modulate the thermostability of microbial esterases from the hormone-sensitive lipase family. J Biol Chem 290:11188–11198

Liu L, Suchard MA, Huelsenbeck JP (2012) MrBayes 3.2: efficient Bayesian phylogenetic inference and model choice across a large model space. Syst Biol 61:539–342

Liu Y, Xu H, Yan Q, Yang S, Duan X, Jiang Z (2013) Biochemical characterization of a first fungal esterase from *Rhizomucor miehei* showing high efficiency of ester synthesis. PLoS One 8:e77856

Lorenz P, Eck J (2005) Metagenomics and industrial applications. Nat Rev 3:510–516

Maester TC, Pereira MR, Machado Sierra EG, Balan A, de Macedo Lemos EG (2016) Characterization of EST3: a metagenomic-derived esterase with suitable properties for biotechnological applications. Appl Microbiol Biotechnol 13:5815–5827

Manco G, Mandrich L, Rossi M (2001) Residues at the active site of the esterase 2 from *Alicyclobacillus acidocaldarius* involved in substrate specificity and catalytic activity at high temperature. J Biol Chem 276:37482–37490

Mandrich L, Merone L, Pezzullo M, Cipolla L, Nicotra F, Rossi M (2005) Role of the N terminus in enzyme activity, stability and specificity in thermophilic esterases belonging to the HSL family. J Mol Biol 345: 501–512

Murshudov GN, Skubák P, Lebedev AA, Pannu NS, Steiner RA, Nicholls RA, Winn MD, Long F, Vagin AA (2011) REFMAC 5 for the refinement of macromolecular crystal structures research papers. Acta Crystallogr D Biol Crystallogr D67:355–367

Nam KH, Kim M-Y, Kim S-J, Priyadarshi A, Kwon ST, Koo BS, Yoon SH, Hwang KY (2009) Structural and functional analysis of a novel hormone-sensitive lipase from a metagenome library. Proteins 74: 1036–1040

Nardini M, Dijkstra BW (1999) α/β hydrolase fold enzymes: the family keeps growing. Curr Opnion Struct Biol 9:732–737

Ngo TD, Ryu BH, Ju H, Jang E, Park K, Kim KK, Kim TD (2013) Structural and functional analyses of a bacterial homologue of hormone-sensitive lipase from a metagenomic library. Acta Crystallogr D Biol Crystallogr 69:1726–1737

Ohara K, Unno H, Oshima Y, Hosoya M, Fujino N, Hirooka K, Takahashi S, Yamashita S, Kasunoki M, Nakayama T (2014) Structural insights into the low pH adaptation of a unique carboxylesterase from *Ferroplasma*: altering the pH optima of two carboxylesterases. J Biol Chem 289:24499–24510

Ollis DL, Cheah E, Cyglerl M, Dijkstra B, Frolow F, Franken SM, Harel M, Remington J, Silman I, Schrag J, Sussman JL, Verschueren KHG, Goldman A (1992) The α/β hydrolase fold. Protein Eng 5: 197–211

Paixão DAA, Dimitrov MR, Pereira RM, Accorsini FR, Vidotti MB, Lemos EGL (2010) Molecular analysis of the bacterial diversity in

a specialized consortium for diesel oil. Rev Bras Ciências Solo 34: 773–781

Palm GJ, Fernández-Álvaro E, Bogdanović X, Bartsch S, Sczodrok J, Singh RK, Bottcher D, Atomi H, Bornscheuer UT, Hinrichs W (2011) The crystal structure of an esterase from the hyperthermophilic microorganism *Pyrobaculum calidifonti*s VA1 explains its enantioselectivity. Appl Microbiol Biotechnol 91:1061–1072

Peng Q, Wang X, Shang M, Huang J, Guan G, Li Y, Shi B (2014) Isolation of a novel alkaline-stable lipase from a metagenomic library and its specific application for milkfat flavor production. Microb Cell Factories 13:1–9

Peränen J, Rikkonen M, Hyvonen M, Kaarianen L (1996) T7 vectors with a modified T7lac promoter for expression of proteins in *Escherichia coli*. Anal Biochem 373:371–373

Pereira MR, Mercaldi GF, Maester TC, Balan A, Lemos EGDM (2015) Est16, a new esterase isolated from a metagenomic library of a microbial consortium specializing in diesel oil degradation. PLoS One 10:e0133723

Quax WJ, Brokhuizen C (1994) Development of a new *Bacillus* carboxyl esterase for use in the resolution of chiral drugs. Appl Microbiol Biotechnol 41:425–431

Rao L, Xue Y, Zheng Y, Lu JR, Ma Y (2013) A novel alkaliphilic *Bacillu*s esterase belongs to the 13(th) bacterial lipolytic enzyme family. PLoS One 8:e60645

Rhee J, Ahn D, Kim Y, Oh J (2005) New thermophilic and thermostable esterase with sequence similarity to the hormone-sensitive lipase family, cloned from a metagenomic library. Appl Environ Microbiol 71:817–825

Ronquist F, Teslenko M, van der Mark P, Ayres DL, Darling A, Höhna S, Larget B, Liu L, Suchard MA, Huelsenbeck JP (2012) Mr-Bayes 3.2: efficient Bayesian phylogenetic influence and model choice across a large model space. Syst Biol 61:539–542

Tamura K, Stecher G, Peterson D, Filipski A, Kumar S (2013) MEGA6: Molecular Evolutionary Genetics Analysis version 6.0. Mol Biol Evol 30:2725–2729

Thompson JD, Higgins DG, Gibson TJ (1994) ClustalW: improving the sensitivity of progressive multiple sequence alignment through sequence weighting, position-specific gap penalties and weight matrix choice. Nucleic Acids Res 22:4673–4680

Wei Y, Contreras JA, Sheffield P, Osterlund T, Derewenda U, Kneusel RE, Matern U, Holm C, Derewenda ZS (1999) Crystal structure of brefeldin A esterase, a bacterial homolog of the mammalian hormone-sensitive lipase. Nat Struct Biol 6:340–345

Winn MD, Ballard CC, Cowtan KD, Dodson EJ, Emsley P, Evans PR, Keegan RM, Krissinel EB, Leslie AG, McCoy A, McNicholas SJ, Murshudov GN, Pannu NS, Potterton EA, Powell HR, Read RJ, Vagin A, Wilson KS (2011) Overview of the CCP4 suite and current developments. Acta Crystallogr D Biol Crystallogr International Union of Crystallography 67:235–242

Yang S, Qin Z, Duan X, Yan Q, Jiang Z (2015) Structural insights into the substrate specificity of two esterases from the thermophilic *Rhizomucor miehei*. J of Lipid Res 56:1616–1624

Zhu X, Larsen NA, Basran A, Bruce NC, Wilson IA (2003) Observation of an arsenic adduct in an acetyl esterase crystal structure. J Biol Chem 278:2008–2014